Supplementary information for

A sensor-adaptor mechanism

for enterovirus uncoating from structures of EV71

Xiangxi Wang[1], Wei Peng[1], Jingshan Ren[2], Zhongyu Hu[3], Jiwei Xu[1], Zhiyong Lou[4], Xumei Li[1], Weidong Yin[3], Xinliang Shen[3], Claudine Porta[2], Thomas S. Walter[2], Gwyndaf Evans[5], Danny Axford[5], Robin Owen[5], David J. Rowlands[6], Junzhi Wang[3], David I. Stuart[2,5], Elizabeth E. Fry[2] and Zihe Rao[1,4]

[1]National Laboratory of Macromolecules, Institute of Biophysics, Chinese Academy of Science, Beijing, 100101, China, [2]Division of Structural Biology, University of Oxford, The Henry Wellcome Building for Genomic Medicine, Headington, Oxford, UK, [3]National Institutes for Food and Drug Control, No. 2, TiantanXili, Beijing 100050, China, [4]Laboratory of Structural Biology, School of Medicine, Tsinghua University, Beijing, 100084, China, [5]Diamond Light Sources, Harwell Science and Innovation Campus, Didcot, OX11 0DE, UK, [6] Institute of Molecular and Cellular Biology and Astbury Centre for Structural Molecular Biology, Faculty of Biological Sciences, University of Leeds, Leeds, UK.

This document includes:

Supplementary Figure 1

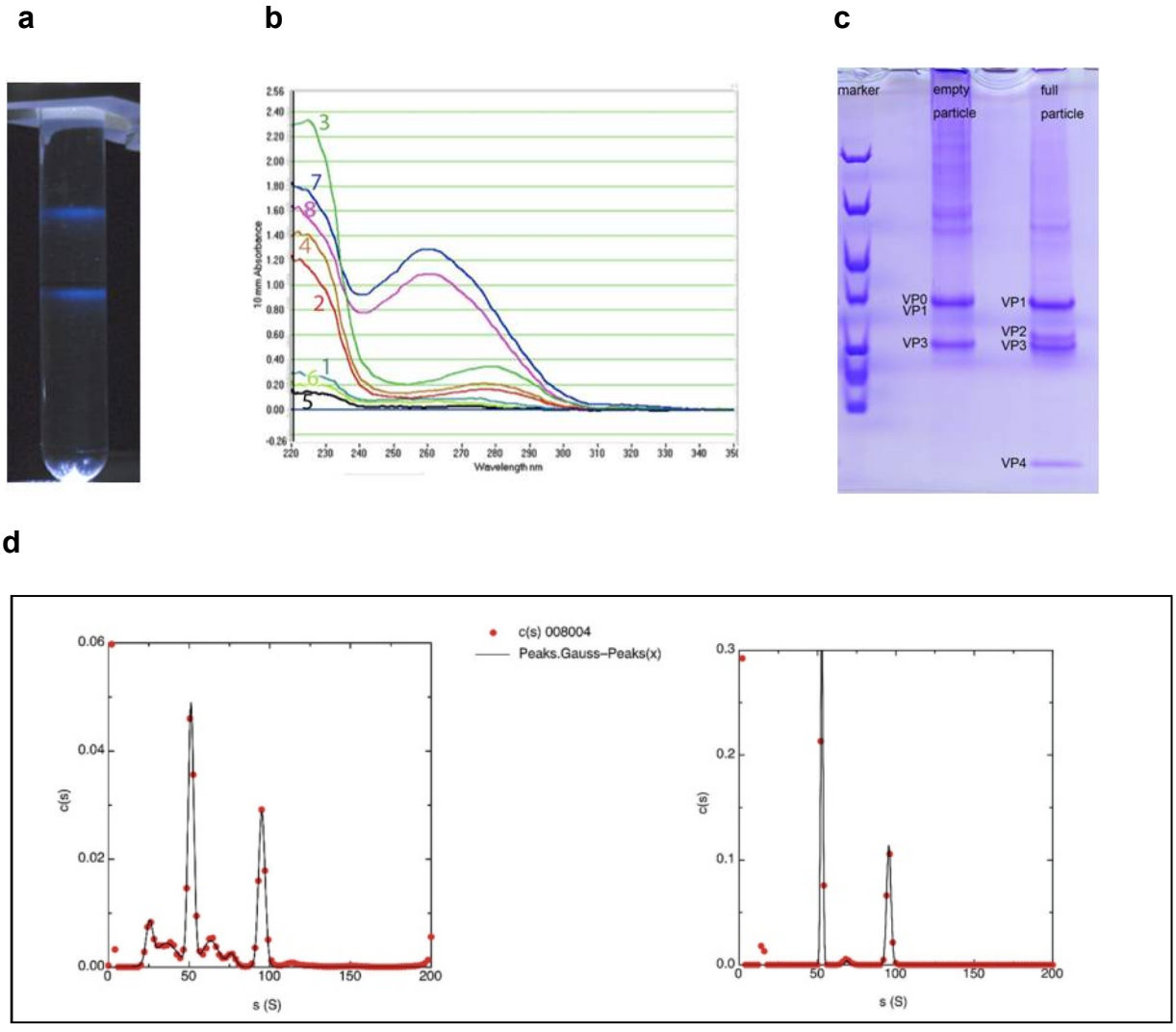

Supplementary Figure 1 EV71 purification**.**

(a) and **(b):** Zonal ultracentrifugation of a 15 to 45% (w/v) sucrose density gradient at 103614g for 3.5 h was used to purify EV71 from the harvest concentrate described in the methods section. Two states of EV71 particle were separated, one band is located one third from the top of the tube containing ~25% sucrose, the other ~33% sucrose. The absorbance ratio (λ260/λ280) of the two states of EV71 virus is quite different, which indicates that the top band (260/280=0.66) are empty particles without the RNA genome and the bottom band (260/280=1.72) are full particles including the RNA genome. **(a)** Shows the gradient, four fractions were collected around each of the two visible bands. **(b)** Shows the absorbance

spectra of the fractions on a Nanodrop spectrophotometer (Thermo Scientific, United States). Note the shift in the absorbance peaks between the two sucrose gradient bands. Fractions 2, 3 and 4 were pooled as empty particles and fractions 7 and 8 as full particles. **(c)** Protein composition of EV71 particles. SDS-PAGE was used to analyze the protein composition of the two particle types isolated as described in Supplementary Figure 1. The figure shows a NuPAGE 4–12% Bis-Tris Gel (Invitrogen). Each lane was loaded with 5-6µg sample. Lane 1 shows markers (molecular weights provided for reference), lane 3 empty particles and lane 5 full particles. The calculated molecular weights of VP0, VP1, VP2, VP3 and VP4 are 35.19kDa, 32.7kDa, 27.7kDa, 26.4kDa and 7.5kDa respectively. The results suggest that empty particles are an immature state of EV71, because they contain VP0 and no VP2. In contrast the full particles contain all four structural proteins VP1, VP2, VP3 and VP4, characteristic of the mature state. Moreover, analysis by MALDI-TOF spectrometry identified the tryptic fragments as human EV71 viral proteins based on sequences in NCBI Entrez (data not shown). Note the evidence of higher molecular weight 'ladders' consistent with some proteins being cross-linked during the formaldehyde inactivation process.

(d) Analytical ultracentrifugation. The sedimentation coefficients for the particles were determined independently for two virus preparations using a virus concentration of 0.3mg mL^{-1} in 0.2M PBS buffer in a Beckman XL-I analytical ultracentrifuge in which the temperature of the rotor was regulated at 4°C to maintain the integrity of the samples. Velocity experiments were performed at 29068g, collecting sample distribution profiles every 5 minutes using absorbance optics with incident light of 300nm and also using interference optics. The data were analysed using the program SedFit[1,2] in c(s) mode to give an apparent distribution of sedimentation coefficients; the 5^{th} to 40^{th} scan were used in each case for the c(s) calculation. The figure shows plots of the apparent c(s) distribution for a series of absorbance scans with the two major peaks having sedimentation coefficients s(T,b) where T is 4°C and b 0.2 M PBS, of 51.2S and 95.1S for the first sample and 52.7S and 95.5S for the second sample. The areas under the Gaussians do not indicate the relative amount of the species since the full particles absorb disproportionately. Correcting these values to the standard s(20,w) using the formula of Tanford[3], gives average values of 81.6 and 149.6 consistent with empty capsids and mature virus particles respectively[4,5].

Supplementary Figure 2

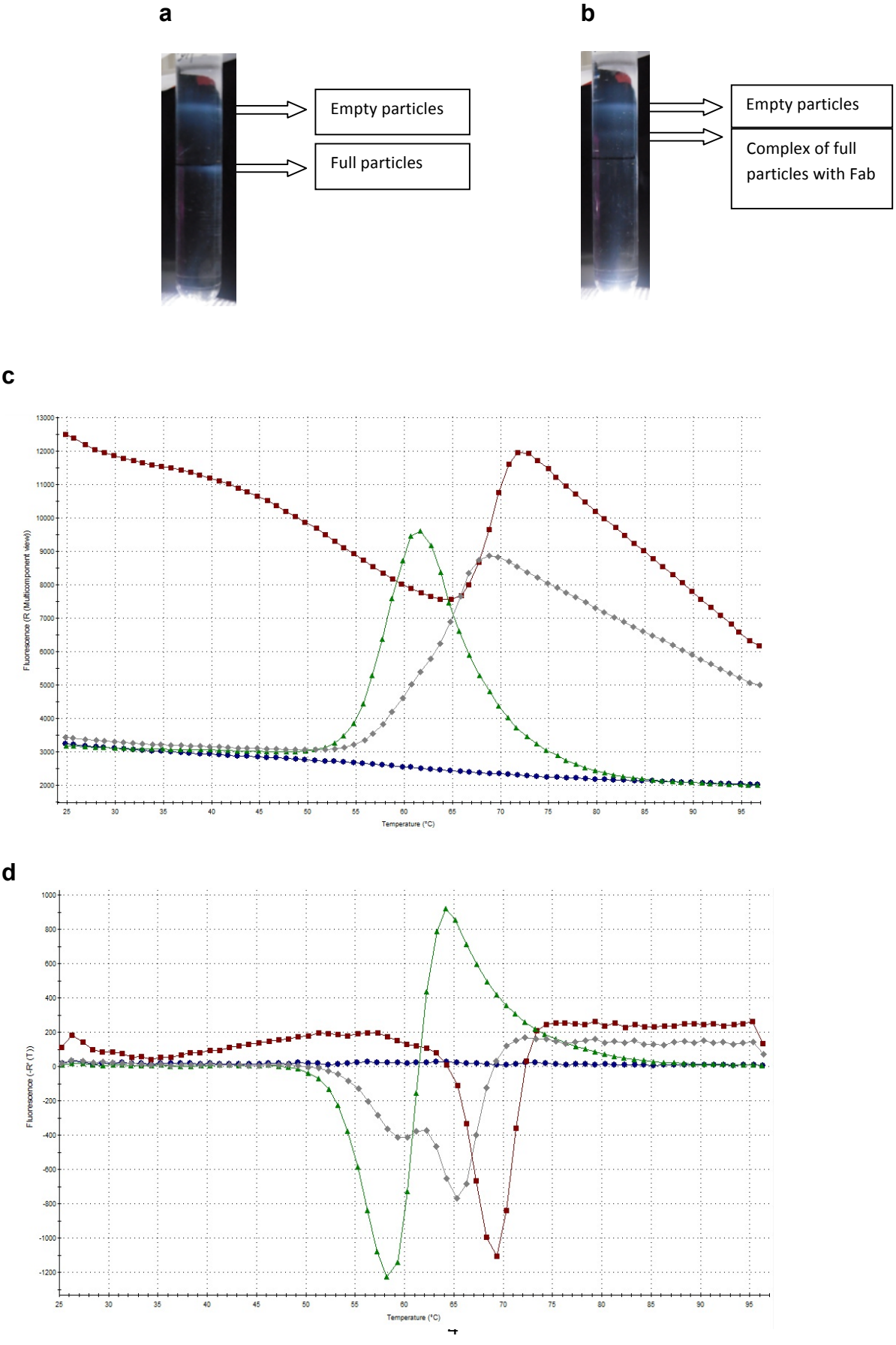

Supplementary Figure 2 EV71 immunogenicity and thermal stability.

(a) and **(b)** Antigenic properties of EV71 full and empty particles. We analysed the interaction of the two types of particle with antibody D6. Generation and purification of Fab fragments from Anti-EV71 monoclonal antibody (mAb) D6 are described in the Online Methods. Interaction between D6 Fab and EV71 virus was analysed by sucrose density gradient ultracentrifugation. The results imply that only EV71 full particles can bind antibody: **(a)** represents the control sample without D6 Fab, the top band is made up of empty particles, the bottom band corresponds to full particles. **(b)** shows an equivalent sample incubated with D6 Fab at 4°C overnight, the top band (still in the same position) consists of EV71 empty particles, indicating no interaction, while the bottom band moves up to a new position, indicating that the full particles are complexed with the D6 Fab.

(c) and **(d)** Thermal stability. To characterize the stability of the two types of EV71 particles, differential scanning fluorimetry assays were performed with dyes SYTO9 (to test for RNA exposure) and SYPRO RED (to test for protein melting). The raw fluorescence traces are shown in (**c**). The blue line represents the result of empty particles incubated with SYTO9, the green line represents that of full particles to which SYTO9 dye has been added, confirming that empty particles contain no detectable RNA, while full particles do contain RNA and release it at ~58ºC. The first derivatives of the fluorescence curves are shown in (**d**). The results with SYPRO RED indicate that empty particles are more stable than full particles (the melting temperature of empty particles is ~ 4ºC higher than that of full particles, red line and grey lines respectively). The higher SYPRO RED fluorescence signal at low temperatures for the empty particles implies that some hydrophobic regions of the particles are solvent exposed. The melting of the mature virus shows two transitions, seen more easily in (**d**), indicating that when the temperature reaches 58ºC, the structure changes coincident with release of the RNA genome, although the particles remain intact, presumably as empty 82S capsids. When the temperature reaches ~65ºC, these particles are lost, as shown by the second transition. This suggests that 82S EV71 empty particles could be produced by careful heating of 150S EV71 full particles.

Supplementary Figure 3

a

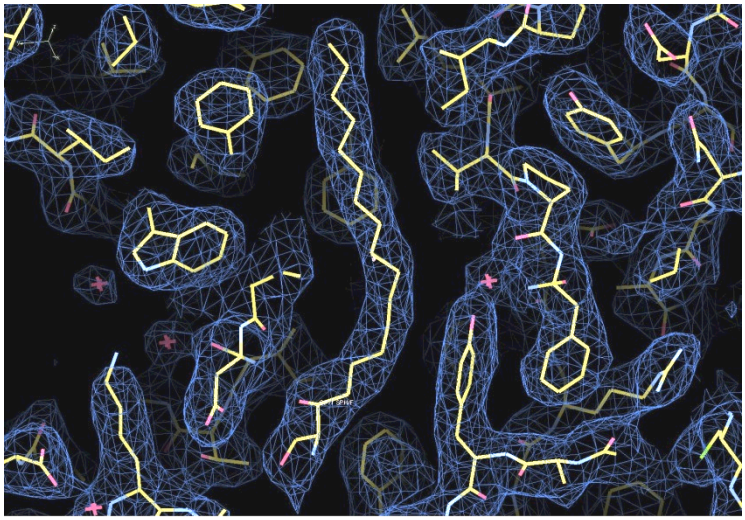

b

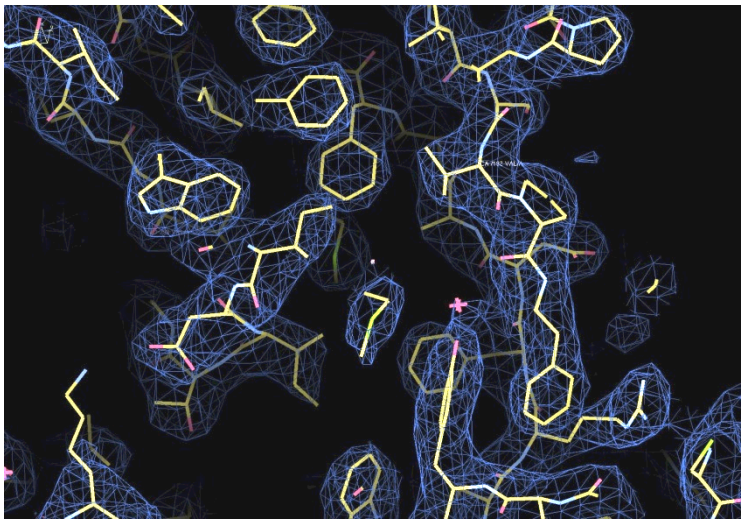

Supplementary Figure 3 Representative electron density.

Representative averaged $|2F_o\text{-}F_c|$ electron density for the mature EV71 virus (space group *R*32) (**a**), and the expanded EV71 particle (collected at 100K) (**b**). Crystallographic statistics for these structures are given in Table 1. The view is similar in both panels. Note the sphingosine 'pocket factor' in the centre of panel **(a)**, in panel **(b)** the pocket has lost the pocket factor, and is largely filled by rearrangements of the polypeptide chain and side chains.

a

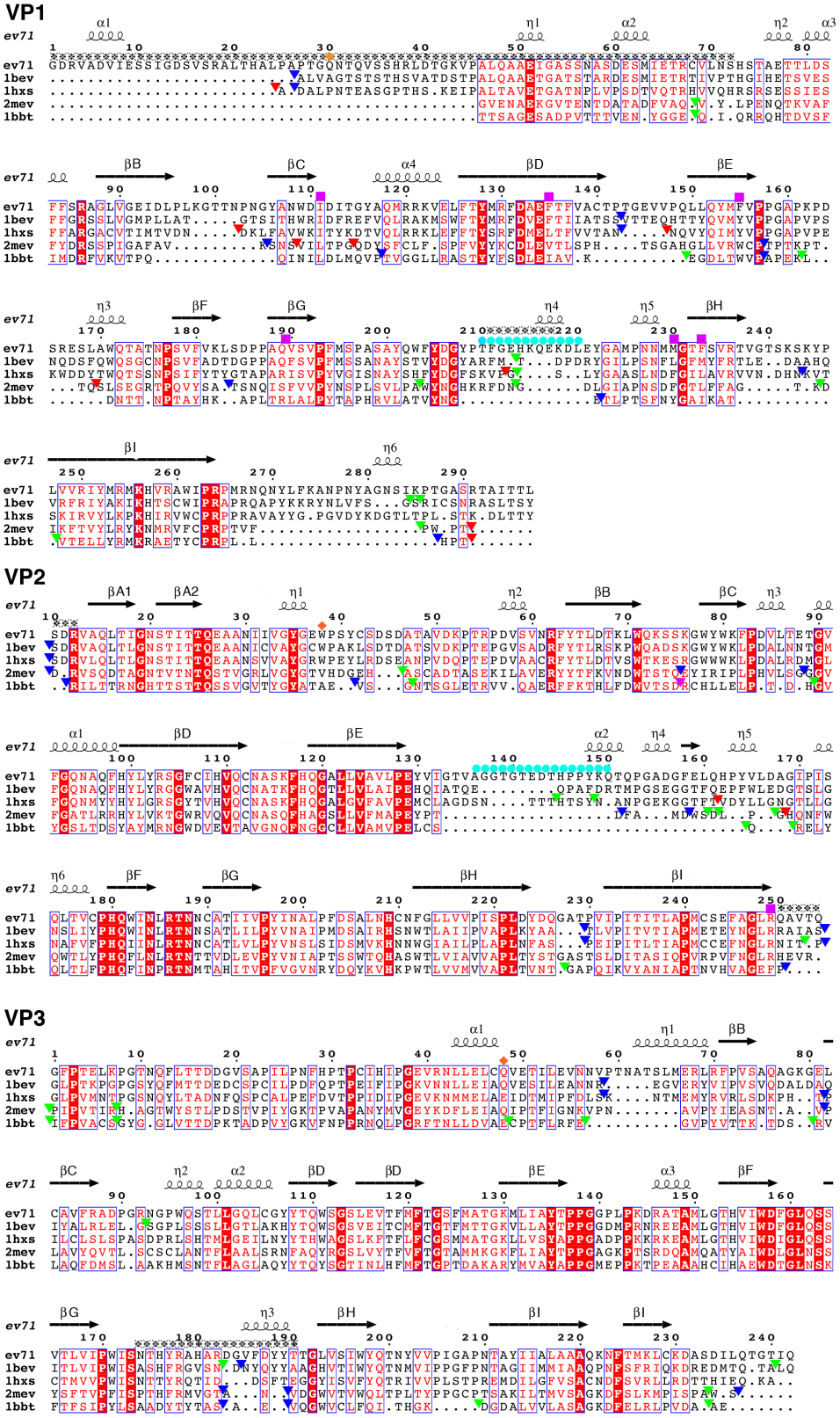

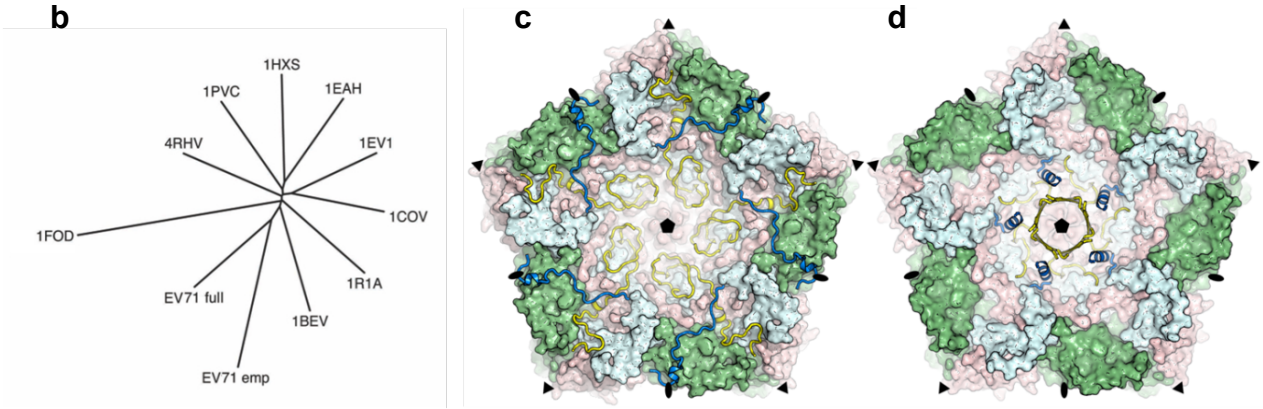

Supplementary Figure 4 Structural comparison of EV71 with other picornaviruses.

(a) Espript[6] representation of a structure-based sequence alignment of VP1, VP2 and VP3 of the mature EV71 particle with representative picornaviruses, namely bovine enterovirus, poliovirus type 1, mengovirus and foot-and-mouth disease virus (PDB codes: 1BEV[7], IHXS[8], 2MEV[9], 1BBT[10] respectively). Since VP4 is extremely structurally variable it was not possible to meaningfully superpose this protein. The secondary structural elements for EV71 are shown, also above the EV71 sequence are symbols which show features described in the text. Cyan spheres mark neutralizing epitope regions, magenta squares mark key residues in the adaptor-sensor region, orange diamonds mark residues apparently interacting with RNA and black flowers show regions disordered in the empty expanded particle (the empty particle contains VP0, which encompasses VP4 and VP2 – the first 81 residues of VP0 are disordered, corresponding to all of VP4 and the first 12 residues of VP2). In order to render the alignment compact, places where there is an insert in one of the other viruses with respect to EV71 are noted by a coloured triangle at the appropriate place above the appropriate sequence. The triangles are colour coded so that the insertion of a single residue is shown in green, a 2-5 residue insertion is shown in blue and a red triangle indicates an insertion of more than 5 residues. The residue numbers are for EV71.

(b) Structure-based phylogenetic tree for representative picornaviruses. The structures chosen are foot and mouth disease virus (O_1BFS) (PDB code: 1FOD[11]), human rhinovirus 14 (4RHV[12]), Sabin strain of type 3 poliovirus (1PVC[13]), Mahoney strain of type 1 poliovirus (1HXS[8]), Lansing strain of type 2 poliovirus (1EAH[14]), echovirus 1 (1EV1[15]), coxsackievirus b3 (1COV[16]), human rhinovirus1A (1R1A[17]) and bovine enterovirus 1 (1BEV[7]). All viruses, with the exception of FMDV (which is included as an outgroup) are entero- viruses. Note that EV71 is most closely related to BEV and that the EV71 expanded capsid (EV71 emp), although most closely related to the EV71 mature virus (EV71 full) is an outlier from all enteroviruses. The analysis was performed using SHP[18] and Phylip[19], in brief the summed structural similarity between pairs of matched residues in each pair of viruses is converted to an evolutionary distance by the use of an empirical logarithmic function, and the full set of pairwise evolutionary distances then visualized as a tree. For each virus a 'biological protomer' (the most structurally coherent arrangement of a single subunit each of VP1-4 which can be extracted from the particle) was used in the analysis.

(c) and **(d)** Unusual structure for the N-termini of VP1 and VP4 in mature particles of EV71. **(c),** compared to **(d)** a more typical enterovirus, human rhinovirus 16 (1AYN[20]). Residues 1-26 of VP1 and all of VP4 for EV71 and residues 1-14 of VP1 and all of the deposited residues of VP4 for HRV16 are shown in cartoon representation, whilst the remaining structure is rendered as a surface. A pentamer of icosahedral protomeric units is shown with the position of the icosahedral symmetry axes shown in black. The colour scheme uses the signature colours (VP1 blue, VP2 green, VP3 red and VP4 yellow). The view is from the inside of the virus.

Supplementary Figure 5

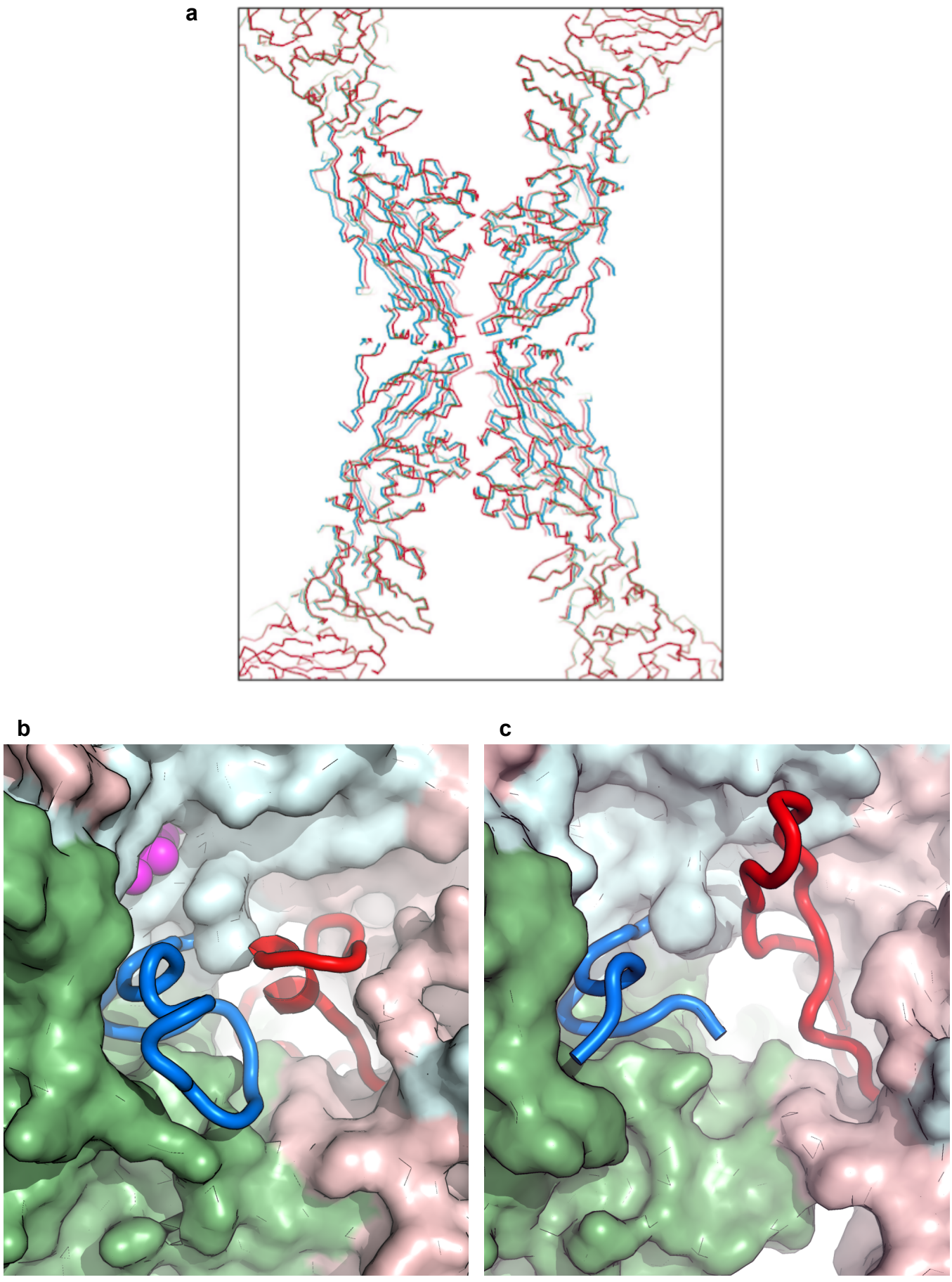

Supplementary Figure 5 Cryo cooling induced distortion of empty particle and changes in the GH loops of VP1 and VP3 upon particle expansion.

(a) Distortion of the expanded empty particle of EV71 upon cooling to 100K. The packing observed in the crystal at 100K is shown in blue (Cα trace representation), note that this structure is non-icosahedral, the effect of introducing icosahedral symmetry (as is seen in the crystal at room temperature) is shown in the red structure. Note that steric clashes are introduced at the interface between the two particles.

(b) and **(c)** Changes in the GH loops of VP1 and VP3 upon particle expansion. Residues VP1 205-225 and VP3 170-192 are shown in cartoon representation whilst the remaining structure is rendered as a surface. The colour scheme uses the signature colours (VP1 blue, VP2 green and VP3 red) with the head group of the pocket factor, visible in panel **(b)** shown in magenta (CPK representation). The view is from the outside of the virus and the orientation is similar to that of **Fig. 1a** in the main paper. Panel **(b)** shows the mature virus and **(c)** the expanded empty particle. Note the hole created in the empty capsid at the base of the canyon by this rearrangement (the VP3 GH loop is very flexible in the expanded particle, having very high B-factors). In addition in panel **(c)** part of the 2-fold hole through the particle is visible at the bottom of the picture.

Supplementary Figure 6

a

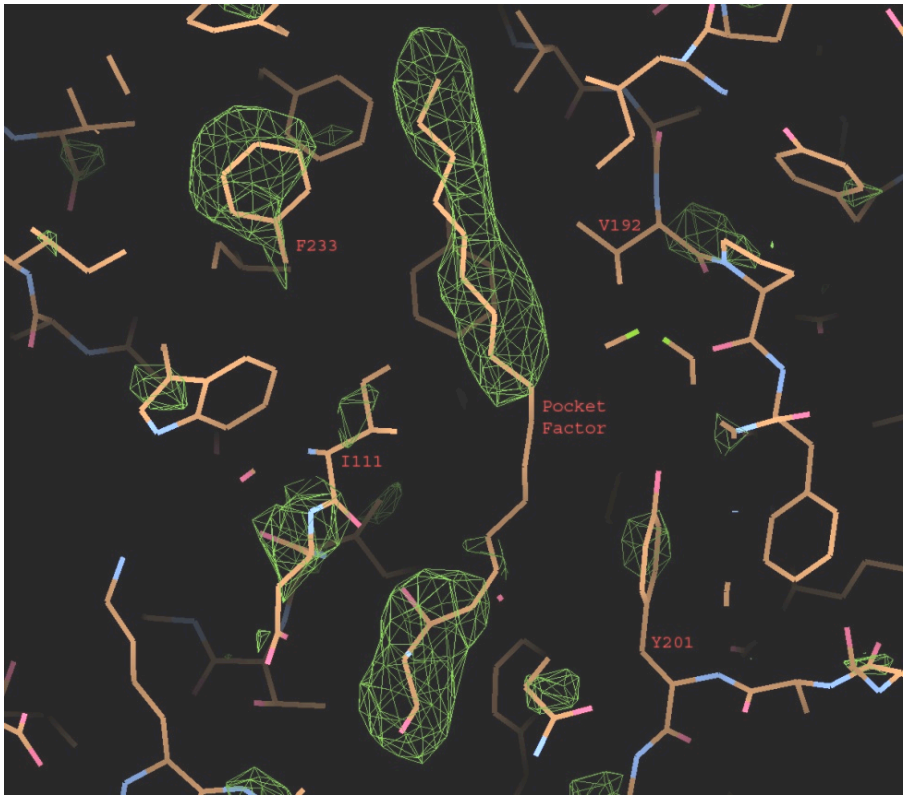

b

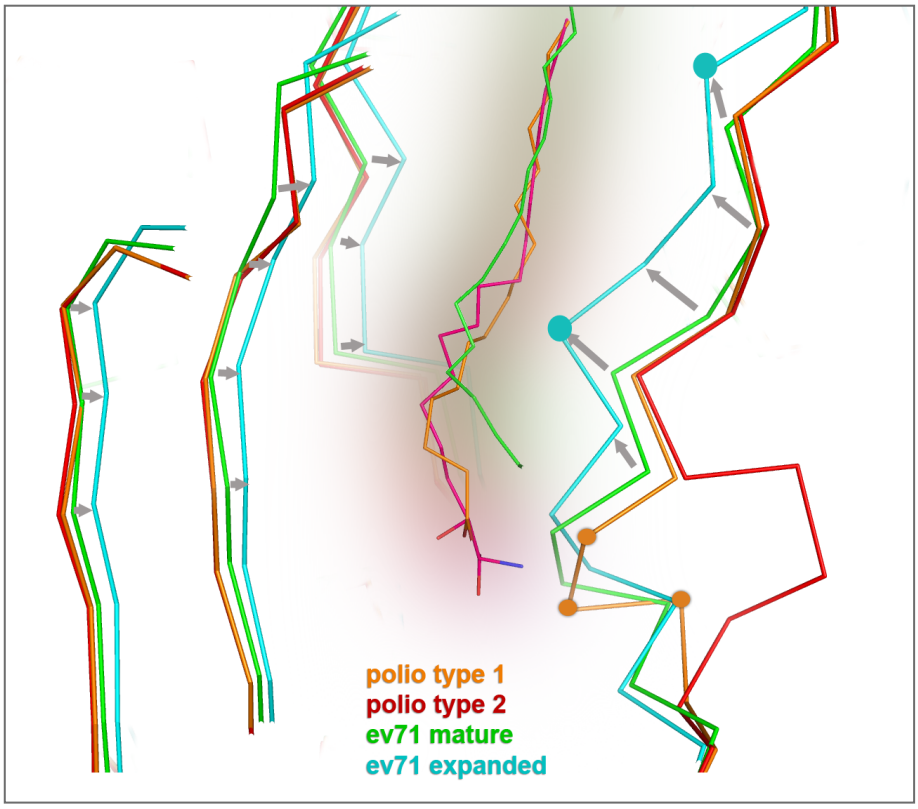

Supplementary Figure 6 Pocket factor binding and adaptor-sensor region.

(a) $|F_o\text{inactive}|-|F_o\text{active}|$ averaged electron density map for the mature virus calculated using the phases of the final refined model of inactivated EV71, contoured at an arbitrary level (the mean-fractional-isomorphous difference between the two data sets is less than 0.2 at low resolution). The positive electron density (shown in green) indicates that the pocket factor in the active virus has a lower occupancy and reflects the conformational change at residue Phe233 that is seen when comparing the mature virus with the expanded empty particle.

(b) A portion of the GH loop adjacent to the adaptor-sensor region is conformationally variable in poliovirus. Four structures are superposed, poliovirus type 1 and 2 (PDB codes 1HXS[8] and 1EAH[14]) and the EV71 mature virus and expanded empty particle. A portion of the VP1 GH loop and strand H is shown to the right of the pocket factors (which possess a coloured glow). The adaptor-sensor (residues 230-233 of VP1 in EV71 - residues 230 and 233 being marked with cyan circles for the expanded particle) is directly C-terminal of three conformationally variable residues in poliovirus (233-235 in type 1 - marked with orange circles). These residues adopt two principle states, ‘up’ and ‘down’. EV71 resembles the down conformation which predominates in poliovirus type 1 (orange). The up conformation is represented by the structure of poliovirus 2 (red). Arrows show the movements which occur on the transition to the expanded particle in EV71.

Supplementary Figure 7

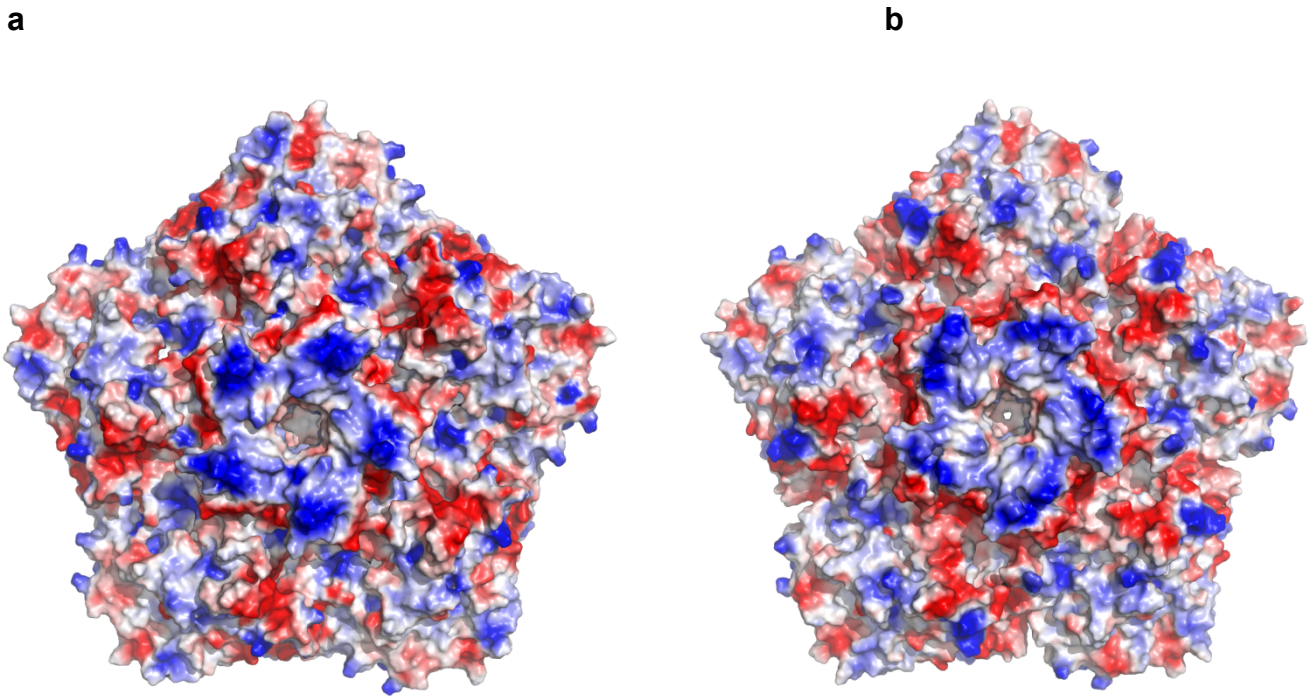

Supplementary Figure 7 Electrostatic surfaces for the two types of EV71 particles.

It is conceivable that EV71 initially attaches to cells via interaction with receptors bearing sugars or sulphated sugars, and there is a coherent area of positive charge adjacent to the 5-fold axes of the virus, whose integrity is disrupted on conversion to the expanded particle, which, by analogy with other picornaviruses[21] would be a likely point of attachment.**(a)** Electrostatic surface of a pentamer from EV71 mature virion, showing strong positively charged patches (blue colour, contributed by conserved Arg166, Lys242 and Lys244, and less conserved Lys98, all from VP1) around the icosahedral 5-fold axis, suggesting a possible receptor binding site. Note that the electrostatic calculations, performed in Pymol, are crude approximations. **(b)** The positively charged patches are altered in the empty particle.

Supplementary Table 1 Protein-protein interactions in mature virus and expanded particles of EV71.

Interface	**Interface Area (A^2); Mature virus → Expanded**
Interface within protomer	
VP1 / VP2	2560 → 1730
VP1 / VP3	3880 → 3000
VP2 / VP3	1570 → 1480
Interface between protomers but within pentamer	
Interface	Interface Area (A^2)
VP1/VP1	850 → 740
VP1/VP2	460 → 0
VP1/VP3	1660 → 1260
VP2/VP3	720 → 350
VP3/VP3	810 → 720
Interface between pentamers	
VP1/VP1	790 → 0
VP1/VP2	1680 → 0
VP2/VP2	690 → 160
VP2/VP3	2600 → 2500
VP3/VP3	90 → 60

References

1. Schuck, P. & Rossmanith, P. Determination of the sedimentation coefficient distribution by least-squares boundary modeling. *Biopolymers* 54, 328-41 (2000).
2. Brown, P.H. & Schuck, P. Macromolecular size-and-shape distributions by sedimentation velocity analytical ultracentrifugation. *Biophys J* 90, 4651-61 (2006).
3. Tanford, C. *Physical Chemistry of Macromolecules*, (John Wiley and Sons, New York, 1961).
4. Brown, F. & Cartwright, B. Purification of radioactive foot-and-mouth disease virus. *Nature* 199, 1168-70 (1963).
5. Rowlands, D.J., Sangar, D.V. & Brown, F. A comparative chemical and serological study of the full and empty particles of foot-and mouth disease virus. *J Gen Virol* 26, 227-38 (1975).
6. Gouet, P., Courcelle, E., Stuart, D.I. & Metoz, F. ESPript: analysis of multiple sequence alignments in PostScript. *Bioinformatics* 15, 305-8 (1999).
7. Smyth, M. et al. Implications for viral uncoating from the structure of bovine enterovirus. *Nat Struct Biol* 2, 224-31 (1995).
8. Miller, S.T., Hogle, J.M. & Filman, D.J. Ab initio phasing of high-symmetry macromolecular complexes: successful phasing of authentic poliovirus data to 3.0 A resolution. *J Mol Biol* 307, 499-512 (2001).
9. Krishnaswamy, S. & Rossmann, M.G. Structural refinement and analysis of Mengo virus. *J Mol Biol* 211, 803-44 (1990).
10. Fry, E., Acharya, R. & Stuart, D. Methods used in the structure determination of foot-and-mouth disease virus. *Acta Crystallogr A* 49 (Pt 1), 45-55 (1993).
11. Logan, D. et al. Structure of a major immunogenic site on foot-and-mouth disease virus. *Nature* 362, 566-8 (1993).
12. Arnold, E. & Rossmann, M.G. The use of molecular-replacement phases for the refinement of the human rhinovirus 14 structure. *Acta Crystallogr A* 44 (Pt 3), 270-82 (1988).
13. Basavappa, R. et al. Role and mechanism of the maturation cleavage of VP0 in poliovirus assembly: structure of the empty capsid assembly intermediate at 2.9 A resolution. *Protein Sci* 3, 1651-69 (1994).
14. Lentz, K.N. et al. Structure of poliovirus type 2 Lansing complexed with antiviral agent SCH48973: comparison of the structural and biological properties of three poliovirus serotypes. *Structure* 5, 961-78 (1997).
15. Filman, D.J., Wien, M.W., Cunningham, J.A., Bergelson, J.M. & Hogle, J.M. Structure determination of echovirus 1. *Acta Crystallogr D Biol Crystallogr* 54, 1261-72 (1998).
16. Muckelbauer, J.K. et al. Structure determination of coxsackievirus B3 to 3.5 A resolution. *Acta Crystallogr D Biol Crystallogr* 51, 871-87 (1995).
17. Kim, S.S. et al. Crystal structure of human rhinovirus serotype 1A (HRV1A). *J Mol Biol* 210, 91-111 (1989).
18. Stuart, D.I., Levine, M., Muirhead, H. & Stammers, D.K. Crystal structure of cat muscle pyruvate kinase at a resolution of 2.6 A. *J Mol Biol* 134, 109-42 (1979).
19. Riffel, N. et al. Atomic resolution structure of Moloney murine leukemia virus matrix protein and its relationship to other retroviral matrix proteins. *Structure* 10, 1627-36 (2002).
20. Oliveira, M.A. et al. The structure of human rhinovirus 16. *Structure* 1, 51-68 (1993).
21. Fry, E.E. et al. Crystal structure of equine rhinitis A virus in complex with its sialic acid receptor. *J Gen Virol* 91, 1971-7 (2010).